Title	Formation of uniform ferrocenyl-terminated monolayer covalently bonded to Si using reaction of hydrogen-terminated Si(111) surface with vinylferrocene/n-decane solution by visible-light excitation.
Author(s)	Sano, Hikaru; Zhao, Mingxiu; Kasahara, Daiji; Murase, Kuniaki; Ichii, Takashi; Sugimura, Hiroyuki
Citation	Journal of colloid and interface science (2011), 361(1): 259-269
Issue Date	2011-09-01
URL	http://hdl.handle.net/2433/143737
Right	© 2011 Elsevier Inc.
Type	Journal Article
Textversion	author

Formation of Uniform Ferrocenyl-terminated Monolayer Covalently Bonded to Si Using Reaction of Hydrogen-Terminated Si(111) Surface with Vinylferrocene/n-Decane Solution by Visible-Light Excitation

Hikaru Sano[1], Mingxiu Zhao[2], Daiji Kasahara, Kuniaki Murase*, Takashi Ichii, Hiroyuki Sugimura

* Corresponding author

Department of Materials Science and Engineering, Kyoto University

Yoshida-hommachi, Sakyo-ku, Kyoto 606-8501, Japan

Tel.: +81-75-753-9132

Fax: +81-75-753-5441

E-mail: murase.kuniaki.2n@kyoto-u.ac.jp

1 Present address

Research Institute for Ubiquitous Energy Devices, National Institute of Advanced Industrial Science and Technology (AIST), Midorigaoka 1-8-31, Ikeda, Osaka 563-8577, Japan

2 Present address

Department of Applied Chemistry, School of Engineering, The University of Tokyo, 7-3-1 Hongo, Bunkyo-ku, Tokyo 113-8656, Japan

Abstract

Electrochemically active self-assembled monolayers (SAM) have been successfully fabricated with atomic-scale uniformity on a silicon (Si) (111) surface by immobilizing vinylferrocene (VFC) molecules through Si-C covalent bonds. The reaction of VFC with the hydrogen-terminated Si (H-Si) (111) surface was photochemically promoted by irradiation of visible light on a H-Si(111) substrate immersed in *n*-decane solution of VFC. We found that aggregation and polymerization of VFC was avoided when *n*-decane was used as a solvent. Voltammetric quantification revealed that the surface density of ferrocenyl groups was 1.4×10^{-10} mol cm^{-2}, i.e., 11% in substitution rate of Si-H bond. VFC-SAMs were then formed by the optimized preparation method on n-type and p-type Si wafers. VFC-SAM on n-type Si showed positive photo-responsivity, while VFC-SAM on p-type Si showed negative photo-responsivity.

Keywords

Self-Assembled Monolayer, Ferrocenyl Group, Vinylferrocene, Electrochemically Active, AFM, Cyclic Voltammetry

1. Introduction

Self-assembling, one of the bottom-up technologies, has attracted much attention due to the desire to control the structure of materials and devices on minute scales. A typical example fabricated with the self-assembly technique is the so-called self-assembled monolayers (SAMs) [1-4], which are ultrathin organic films with a uniform mono-molecular thickness. When you put a certain set of precursor molecules and a substrate into a reaction cup, the molecules chemisorb on the substrate surface, and are spontaneously arranged with their reactive site facing the surface. During the chemisorption process, the molecules are assembled with a highly oriented arrangement due to intermolecular interactions. The resulting organic film is immobilized on the surface through chemical bonds, and hence is fairly stable compared with other types of organic monolayers, e.g., Langmuir-Blodgett films [1,4].

To hybridize organic and inorganic materials, the formation of a SAM on the inorganic substrate surface is of primary importance [5-8]. It is well known that organosilane molecules form SAMs on silicon (Si) substrates through silane coupling chemistry [7]. In this case, precursor organosilane molecules react with native oxide on the Si substrate. Accordingly, an insulator layer is inevitably present between the SAM and the bulk Si. This intermediate insulator layer prevents the electrical link between the organic and the inorganic materials. However, from the view point of the electrical integration of the two materials, a direct connection between SAMs and Si substrates is crucial.

In 1993, Linford et al. [9] reported on a direct conjugation method of SAM and Si substrate, using diacyl peroxides and hydrogen-terminated Si (H-Si) substrate. They employed the thermal decomposition of diacyl peroxides in order to generate alkyl radicals. Here, the radicals react with the H-Si surface and extract H atoms from the surface, yielding Si dangling bonds, i.e., Si radicals, on the surface. Each Si dangling bond further reacts with an alkyl radical to form an alkyl group covalently bonded to Si, so a SAM is formed on the surface with interfacial linkages of Si-C. In this system, the SAMs are directly immobilized on the Si surface; hence this can be a key technology for future hybrid devices. In 1995, the same group reported that 1-alkene served as a precursor to form the *"directly bonded SAM"* without the radical generator through a proper thermal treatment [10]. So far, similar SAMs have been reported by many groups [11-23]. Precursor molecules such as 1-alkenes, 1-alcohols, *n*-aldehydes, and 1-amines react with H-Si substrates through heat treatment, UV irradiation, visible light irradiation [17-23], and combinations of these processes. Our group has also examined SAM formation from 1-hexadecene through heat treatment, UV irradiation, and visible light irradiation, and found that all three processes provided equivalent SAMs from the viewpoint of physical properties, and maintained the atomically flat feature of H-Si(111) surface [22]. In this report, the mechanism of SAM formation by visible light irradiation method is suggested: Light irradiation on the silicon surface creates electrons and holes in the bulk, which are separated by the electric field typically found in the subsurface space charge region. The hydrogen-terminated n-type silicon samples exhibit upward band-bending near the surface, such that photoexited electrons drift into the bulk and photoexited holes drift towards the surface, where they can induce reactions of a nucleophilic vinyl group with the H-terminated surface. The

carbon-carbon double bond of a 1-alkene approaches the Si-H bond in a parallel fashion, and they then form a four-membered transition state, resulting in the evolution of a Si-C bond. Additionally, for the case of hydrogen-terminated p-type silicon samples, downward band-bending is generated near the surface and nucleophilic vinyl groups are unlikely to attack the surface, so the SAM formation rate is relatively slow or the SAM coverage is relatively small.

A SAM with redoxactivity is of special interest for application in future electronic devices, since such a SAM can store charges and serve as a molecular memory unit [24-30]. When redox-active molecules are used as precursors of directly bonded SAMs, as in the case of 1-alkenes with a redox-inert carbon chain, the redox-active moieties are expected to assemble with the molecular-level uniformity, which level is required for future minute electronic devices. However, it is quite difficult to prepare uniform SAMs of redox-active molecules connected to an Si surface with direct bonds, because precursor molecules with a redox-functional group are generally easily damaged by the treatment to promote the reaction of the molecule with the surface. Although there have been many reports on the attachment of redox-active molecules on Si [24-28,31-48], only Fabre et al. have reported clear evidence that ferrocenyl molecules, the redox activity of which is well known, forms a uniform monolayer with an atomic-level flatness [48]. They avoided the damage on the redox-active moieties by a process with the following complicated steps: (*i*) Formation of an ester-terminated SAM on a H-Si substrate; (*ii*) Decomposition of the ester moieties into carboxylic groups in a basic solution, yielding a carboxy-terminated surface; (*iii*) Activation of the carboxy-terminated surface through reaction with

N-hydroxysuccinimide in the presence of a dehydration condensation agent; and (*iv*) Reaction of the activated surface with aminoferrocene. Using this method, ferrocenyl molecules, which are known to show a stable redox behavior and are frequently used in electrochemical experiments, were treated under gentle conditions so that they did not decompose. The resulting film was quite uniform and flat as confirmed by atomic force microscopy (AFM). Although they succeeded in fabricating ferrocenyl-terminated SAM with the above four-step SAM formation process, it is known that the surface roughness increases when monolayers are stacked in layers [49]. A rough surface may pose an impediment when minimizing the size of devices built with this process.

In contrast, we aim to fabricate ferrocenyl-terminated SAM with a simple one-step SAM formation process. At the same time, we also focus on the visible light irradiation method, which condition is so gentle that the ferrocenyl moieties should not be damaged. Vinylferrocene was used as a precursor and H-Si(111) as a substrate. The advantage of vinylferrocene is that each ferrocene moiety in the resulting SAM is connected to Si through a simple chemical structure, that is, one ethylene unit. This would afford simplicity when the electronic properties of this ferrocene-Si system are discussed. In order to obtain more uniform SAMs, we compared the visible light irradiation method with the heating method. We chose mesitylene as a solvent, since Sieval et al. have reported low alkene concentrations can be used to form well ordered monolayers on the H-Si surface only in mesitylene solution [14]. As is described in the Results and discussion, mesitylene solution does not works well in the case of VFC as solute. Then we focused on the *n*-decane as a solvent, since Sieval et al. [14] have

reported that *n*-decane solution can be used to form SAMs and the molecular structure of *n*-decane is much different from that of mesitylene. Further explanation on this point will be given in the Results and discussion. In the present study, we compared mesitylene with *n*-decane. After optimizing the preparation method, the photo-responsivity of the SAM-formed sample with both n-type and p-type Si wafers was investigated. The photo-responsivity is important to expand the potential for realizing optical devices with such electro-active monolayers.

2. Experimental methods

2.1 Hydrogen-termination

A Si(111) wafer (Arsenic doped, n-type, 0.001 - 0.004 Ω cm, single-side mirror-polished) was used for the present experiments. All the substrates cut from the wafer were cleaned ultrasonically with ethanol and ultrapure water (> 18.0 Ω cm) and then photochemically cleaned by exposing to vacuum ultraviolet generated from a xenon excimer lamp (172 nm, 10 mW cm^{-2}) for 20 minutes [50]. H-Si substrates were obtained by etching the cleaned samples in 5% HF solution (diluted from 50% HF aqueous solution, Morita Chemical, semiconductor grade) for 30 sec at room temperature and subsequently in 40% NH_4F solution (Daikin, semiconductor grade) for 60 sec at 80 °C [51]. During the HF treatment, the experimental set up was covered with an aluminum light shield. The NH_4F solution was heated up to 80 °C to remove the dissolved oxygen. The native oxide layer on each sample was removed and the surface Si atoms were terminated with hydrogen for all these treatments.

2.2 Sample preparation

Vinylferrocene (VFC, Tokyo Chemical Industry, >97%) was used as a precursor molecule without further purification. Hydrosilylation, the reaction of the vinyl group in VFC with Si-H bond on the H-Si surface in this case, was performed under two different activation methods, heating and visible light irradiation, as summarized in Table 1.

Table 1 Conditions for the reaction of vinylferrocene (VFC) with hydrogen-terminated Si(111) surface.

Sample name	Activation method	Temperature or light intensity	Reaction time	Concentration of VFC	Solvent
HM sample	Heat	150 ˚C	2 h	10 mM	Mesitylene
HD sample	Heat	150 ˚C	2 h	10 mM	*n*-Decane
LM sample	Light	510 mW cm^{-2}	2 h	10 mM	Mesitylene
LD sample	Light	510 mW cm^{-2}	4 h	10 mM	*n*-Decane

The thermal activation system consisting of a three-necked separable glass flask equipped with a thermometer, an Allihn condenser for refluxing, and a N_2 gas inlet, was set on a hot plate. 10 mM (M = mol dm^{-3}) mesitylene (Nacalai Tesque, 98%) or *n*-decane (Aldrich, ≥99%) solution of VFC was put in the flask. In order to suppress oxidation of the H-Si substrate surface by dissolved oxygen, deaeration was carried out for at least 30 minutes before and after the freshly prepared H-Si was immersed in the solution and the deaeration was continued during the reaction. The solution was heated up to 150 °C and was kept for 2 h. Heating temperature are set to be just below

the boiling point (b.p.) of the solvents; b.p. of mesitylene is 165 ˚C and b.p. of *n*-decane is 174 ˚C. After film formation with the heat activation method, the samples were subsequently sonicated for 10 minutes each in *n*-hexane, methanol, and ultrapure water, in that order.

A custom-made quartz vessel was used for the visible light activation method. The main part of the vessel was a rectangular cell (thickness 5 mm, width 20 mm, length 45 mm) attached to one end of a cylindrical quartz tube with a diameter of 20 mm; the capacity was about 100 cm^3 in total. 10 mM mesitylene or *n*-decane solution of VFC with volume of about 50 cm^3 was put into the vessel. An inlet and outlet of N_2 gas were attached using a silicone rubber stopper inserted at the open end of the cylinder. The solution was deaerated for at least 30 min, and then a H-Si substrate was quickly slipped into the rectangular cell. The substrate was irradiated with a xenon lamp [Asahi Spectra, MAX-1000 (UV-lamp + vis-mirror)] from the outside of the cell. Light with wavelengths longer than 850 nm was cut off by the vis-mirror. The spectrum of the light irradiated from the optical fiber is shown in Figure 1. The intensity, i.e. absolute irradiance, of the visible light was controlled at 510 mW cm^{-2} by using a neutral density filter installed inside the xenon lamp source. Light intensity was decided to be as high as we can obtain steadily with the machine in our laboratory. As is described in the latter part of Results and discussion, a SAM film was also obtained with rather lower light intensity of 170 mW cm^{-2}. After film formation with the visible light activation method, the samples were sonicated for 10 minutes each in *n*-hexane, methanol, and ultrapure water, in that order.

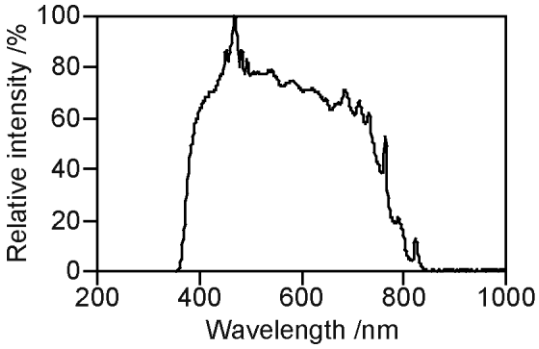

Figure 1 The spectrum of the visible light irradiated from the optical fiber used for the visible light irradiation for SAM formation in the present study.

The resulting samples are hereafter referred to as HM, HD, LM, and LD samples corresponding to the names in Table 1 (e.g. HM = heating - mesitylene). Alkene SAMs are formed in several hours in ordinary cases [11-23], but decomposition or polymerization are observed for 2 hours under HD, HM, and LM conditions. Under the these conditions, decomposition or polymerization is more dominant than SAM formation.

2.3 Analytical tools

The static water contact angles of the samples were measured with water droplets of fixed size about 1.5 mm in diameter.

X-ray photo-electron spectroscopy (XPS) analysis was carried out using an ESCA-3400 system (Kratos Analyical), the background pressure of which was lower than 5×10^{-6} Pa during analysis. The X-ray source was Mg-Kα operated at 10 kV and 10 mA. The Fe 2p, O 1s, C 1s, and Si 2p regions were scanned for all the samples

under the conditions 0.1 eV of step width, 298.5 ms of sampling time, and 10 scan cycles, except that in the Fe 2p region a 170.9 ms of sampling time was used. Gaussian-Lorentzian peak deconvolution and fitting were performed for qualitative and quantitative analysis of the spectra after subtraction of each background.

The thicknesses of the organic film on the Si sample were measured with a spectroscopic ellipsometer (Otsuka Electronics, FE-5000). The measured region was 400 to 800 nm in wavelength and the incident angle was set to be 70°. The model of air / organic film / Si was used for the analysis of raw data. The refractive index of SiO_2 [52] was used as an alternative to the true index of the organic film for all the measured wavelengths; this alternative is usually used for the ellipsometric analysis of self-assembled alkyl monolayers. Actually, VFC film must have a refractive index different from that of SAMs consisting mainly of carbon chains. Thus, in our case, the calculated thicknesses are not the absolute values, and we used them for relative comparison. Topographic images of the resulting samples with an area of 500 nm × 500 nm were acquired by an AFM (Seiko Instruments, SPA-300HV + SPI-3800N) using Si probes with a tip radius of about 15 nm.

Cyclic voltammetry (CV) was carried out at room temperature in the dark or under room lighting with a conventional three-electrode setup connected to an electrochemical analyzer (BLS, ALS 660C). A cylindrical glass cell with a silicone rubber lid was used as the electrolytic vessel. The electrolyte used was 0.1 M $HClO_4$ aqueous solution purged with nitrogen gas before and during the voltammetry. The resulting samples were used as the working electrode. A small copper plate with a

coated copper lead wire was attached to the scratched backside of the substrate on which a gallium-indium eutectic was pasted so that ohmic contact would be obtained at the Si/copper interface. An insulating epoxy resin was then applied to the whole backside and lateral side of the substrate, so that only the front face with a fixed area (1 × 2 cm) was exposed to the electrolyte and was the reactive area during the CV measurement. A coiled platinum wire washed with dilute nitric acid was used as the counter electrode. An Ag/AgCl electrode, immersed in 3.0 M NaCl aqueous solution and fitted with a ground glass liquid junction, was used as the reference electrode. The potential of the reference electrode was 0.226 ± 0.004 V versus standard hydrogen electrode (SHE) [53]. Here we have to note that the filling solution of the reference electrode should not be the commonly-used KCl solution but NaCl solution to avoid the precipitation of the poorly-soluble salt $KClO_4$ at the liquid junction. Low-pass filters with cutoffs at 1.5 Hz and 15 Hz were used to smooth the raw CV data for scan rates of 0.01 to 0.05 V s^{-1} and 0.1 to 0.5 V s^{-1}, respectively.

3. Results and discussion

3.1 Difference in film formation method

The water contact angles, XPS quantitative analytical data, and ellipsometric thicknesses of four samples after film formation are summarized in Table 2 and XPS Fe 2p spectra of four samples are shown in Figure 2; the data for H-Si substrate before film formation are also shown. The water contact angle of H-Si was 85.4˚ and agrees with the reference data [22,54]. In Figure 2, each spectrum of film-formed samples has two large peak contributions around 708.0 eV of binding energy and at about 720.9 eV. These results are consistent with other referenced data [55] and imply that VFC

molecules are immobilized on the substrate in any form. The former peak and the latter peak are attributed to be Fe $2p_{3/2}$ and Fe $2p_{1/2}$. These peaks for HM and HD samples have their shoulder peak at rather higher binding energies. These shoulder peaks come from three-valenced Fe and the main peaks come from two-valenced Fe. In contrast, for LM and LD samples, there are slight contributions from three-valenced Fe. The two-valenced Fe signal component implies the existence of Fc^{0+} and the absence of a three-valenced Fe signal component implies no Fc^{1+} or iron oxide (Fe_2O_3). In the XPS quantitative analysis shown in Table 2, the low carbon and oxygen densities around 3 at.% also suggest successful hydrogen-termination. After film formation, we observed the existence of Fe atoms of 1.4 to 1.9 at.% and an increase in C atoms for all samples by XPS measurement. This means that the VFC molecules were strongly absorbed on the H-Si surface and were not removed by sonication, probably indicating that the VFC molecules are not physisorbed but chemisorbed on the surface. It is considered that the increases in the Fe and C amounts are due to the attachment of VFC and, if this is the case, the C / Fe ratios of the samples should be equivalent to that of VFC molecule, i.e., 12. The estimated C / Fe ratios are listed in Table 2; here, the ratios were calculated by subtracting the C value of the H-Si sample as a background. For HM and HD samples, the ratios of 24.7 and 16.1, respectively, are larger than the ideal value of 12, implying that VFC molecules in these cases were not deposited on the substrate surface in its original form. Further discussion on this will be presented later after considering the results of AFM and CV measurements. The increase in the O amount more likely corresponds to the oxidation of attached VFC molecules or of the Si substrates. We also discuss this later with the results of thickness.

Table 2 Water contact angles, XPS quantitative analytical data, and ellipsometric thickness of hydrogen-terminated silicon and four samples after film formation.

	Water contact angle [˚]	XPS quantitative analysis [at.%]					
		Fe	C	O	Si	C / Fe ratio	Ellipsometric thickness [nm]
H-Si sample	85.4	—	2.5	3.1	94.4	—	—
HM sample	56.0	1.9	49.5	14.6	34.0	24.7	4.87
HD sample	64.0	1.8	31.5	16.6	50.1	16.1	3.81
LM sample	60.6	1.4	18.4	18.6	61.6	11.4	1.93
LD sample	75.6	1.5	17.5	12.8	68.2	10.0	1.75

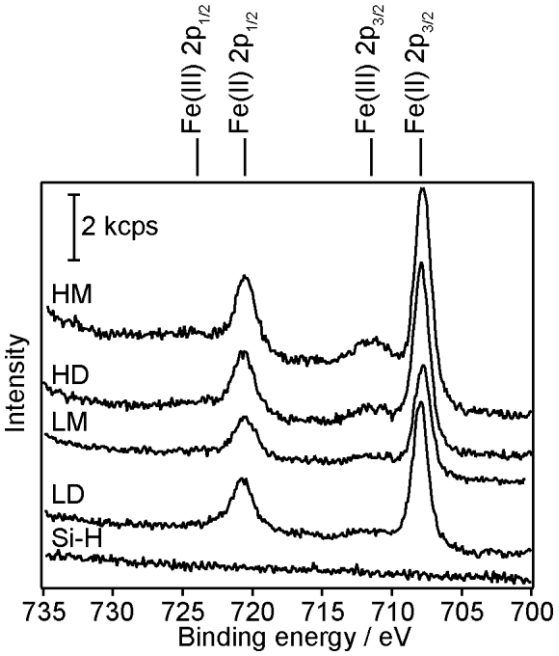

Figure 2 XPS Fe 2p spectra of samples after the reaction with vinylferrocene (VFC) by (HM, HD) heating method or (LM, LD) light irradiation method, with reference data

of hydrogen-terminated Si(111) substrate. The solvent to dissolve VFC was (HM, LM) mesitylene or (HD, LD) *n*-decane.

AFM topographic images of the four samples together with H-Si are displayed in Figure 3. The surface of H-Si had a stair-like structure consisting of monoatomic steps and atomically flat terraces (Figure 3a). This stair-like structure is very typical for the H-Si(111) surface treated with NH_4F solution or buffered HF solution [13,56]. As shown in Figures 3b and 3c, the surfaces of HM and HD samples showed a particulate feature and the stair-like structure had disappeared, indicating that VFC molecules aggregated on the sample surfaces. Here, we should note that the AFM probe used for imaging has a tip radius of about around 20 nm, hence the particle diameter in the AFM images does not reflect the real value that must be smaller due to the so-called tip effect. We thus focused on the height of these particles on HM and HD samples, which were around 12 nm and 2 nm, respectively. In contrast, the samples prepared by the visible light irradiation method, i.e., LM and LD samples, had much fewer and smaller particles on their surfaces. Hence, the stair-like structure of the H-Si substrate was preserved even after the film formation. The size, i.e. height, of the particles was around 1 nm or smaller. Notably, the particles were rarely recognized on the LD sample surface. As summarized in Table 2, the deposits on HM and HD samples contained many more carbon atoms than the expected ratio where VFC molecules are immobilized without large conformation change. Thus, the particles are most likely to be the aggregation of decomposed, or polymerized, VFC molecules, or both. These results are in agreement with the thickness data obtained by ellipsometry; a particulate surface, that is, a rough surface, makes the ellipsometric thickness larger.

However, the thicknesses obtained from the ellipsometric measurement are not absolute values, and can only be used for relative comparison as described in the experimental section.

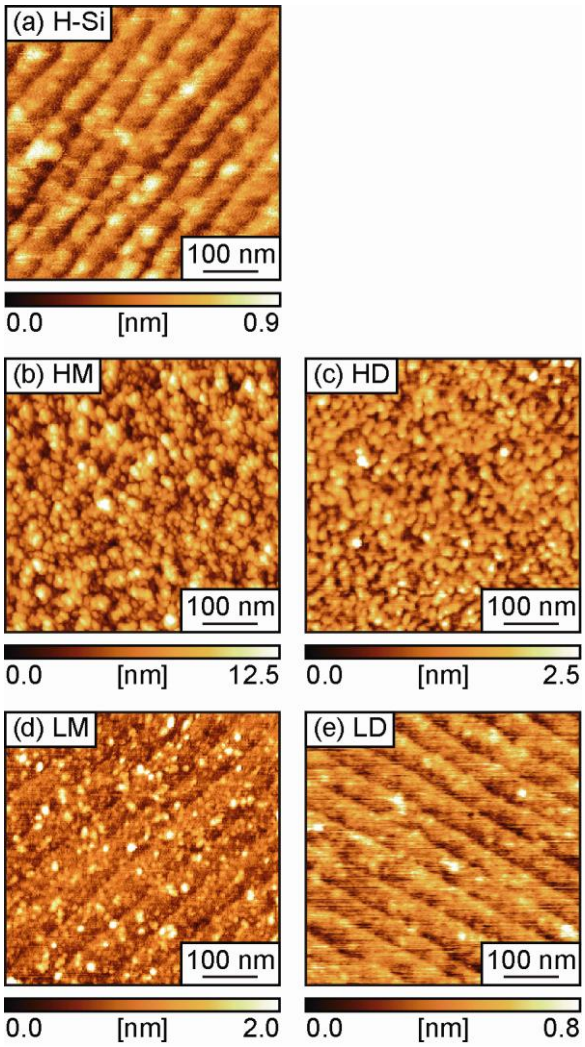

Figure 3 AFM topographic images of (a) hydrogen-terminated Si(111) substrate and samples after the reaction with vinylferrocene (VFC) by (b,c) heating method or (d,e) light irradiation method. The solvent to dissolve VFC was (b,d) mesitylene or (c,e) *n*-decane.

The cyclic voltammograms (CVs) of the four samples are shown in Figure 4. The potential was swept at six different rates ranging from 0.01 to 0.5 V s^{-1}. Pairs of anodic and cathodic waves were observed for each sample, demonstrating that the VFC molecules attached were electrically connected to the Si substrate, keeping their electrochemically active nature to some extent. The anodic peaks for HM sample were located in the range of +0.36 to +0.39 V *vs*. Ag/AgCl (in 3.0 M NaCl), depending on the sweep rate; the anodic peak potential shifted to become more positive with a sweep rate increase. The resistivity of the Si substrate was quite low, 0.001 - 0.004 Ω cm, hence an IR drop within the substrate was not the cause of this peak potential shift. As described above, the results of AFM, XPS, and ellipsometry indicated that aggregation of VFC molecules occurred in this sample. In such a situation, when VFC molecules on the sample are oxidized to the ferricinium (ferrocenium) form that is positively charged, anions have to diffuse or to penetrate into the aggregation layer in order to compensate for the positive charges generated in the film. This diffusion into the aggregation portion is considered to be slower than that in solution, and thus causes a peak shift due to diffusion resistance. The cathodic peaks for HM sample were located at +0.27 V, and the peak separation between the anodic and cathodic peaks lies at around 0.10 V. This peak separation also indicates that the redox involves some diffusion processes. However, both anodic and cathodic peak currents exhibited linear dependencies on the scan rate, as shown in Figure 5a, indicating that the redox systems concerned were confined to the surface and were unrelated to any diffusion process. This result conflicts with the above discussion on peak shift and peak separation. The reason for the discrepancy is unclear, but we think that the contribution of diffusion

during the redox is not so large. The full widths at half-maximum (FWHMs) of the cathodic peaks for HM sample were around 0.25 V, which is broader than the ideal case (i.e., 90.6 mV [57]) of the surface-tethered redox couple with negligible mutual interaction. This peak broadening was due to the repulsion among the positively charged ferricinium moieties when oxidized.

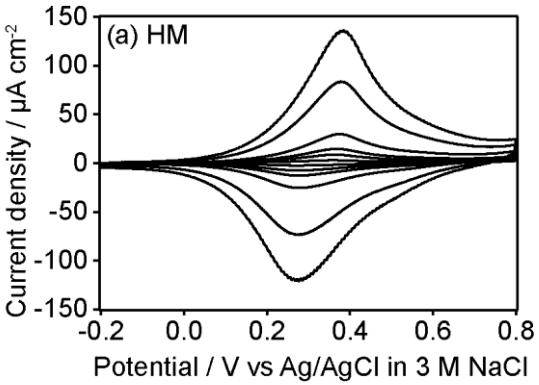
(a) HM
Current density / µA cm-2
150
100
50
0
-50
-100
-150
-0.2
0.0
0.2
0.4
0.6
0.8
Potential / V vs Ag/AgCl in 3 M NaCl

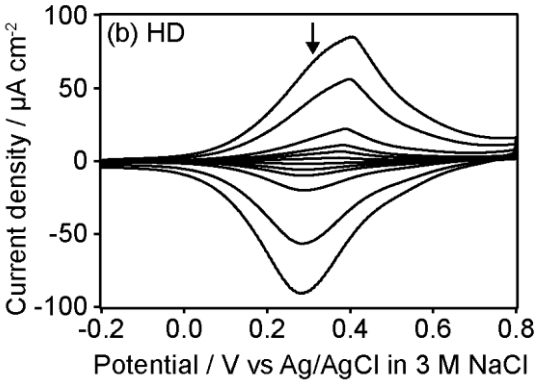
(b) HD
Current density / µA cm-2
100
50
0
-50
-100
-0.2
0.0
0.2
0.4
0.6
0.8
Potential / V vs Ag/AgCl in 3 M NaCl

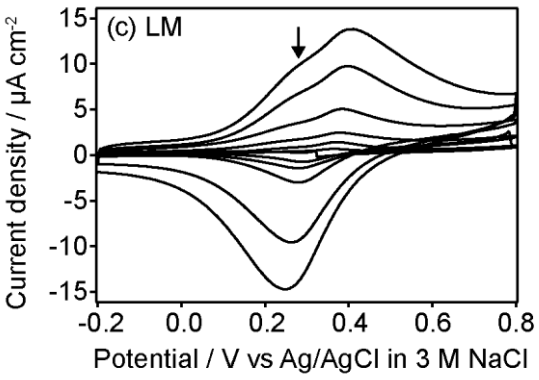
(c) LM
Current density / µA cm-2
15
10
5
0
-5
-10
-15
-0.2
0.0
0.2
0.4
0.6
0.8
Potential / V vs Ag/AgCl in 3 M NaCl

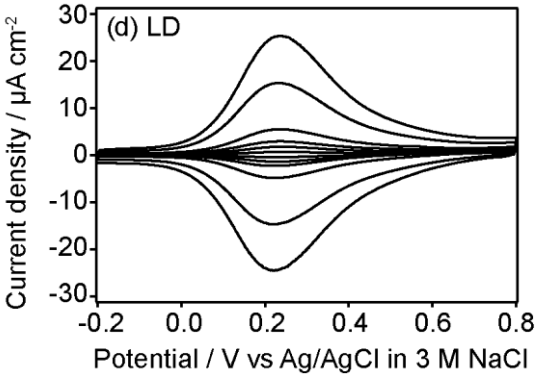
(d) LD
Current density / µA cm-2
30
20
10
0
-10
-20
-30
-0.2
0.0
0.2
0.4
0.6
0.8
Potential / V vs Ag/AgCl in 3 M NaCl

Figure 4 Cyclic voltammograms for hydrogen-terminated Si(111) substrate after the reaction with vinylferrocene (VFC) by (a,b) heating method or (c,d) light irradiation method. The solvent to dissolve VFC was (a,c) mesitylene or (b,d) *n*-decane. The voltammograms were measured in aqueous 0.1 dm^{-3} $HClO_4$ solution at room temperature (a,b) in the dark or (c,d) under room lighting, and scan rates were 0.01, 0.03, 0.05, 0.1, 0.3, and 0.5 Vs^{-1}.

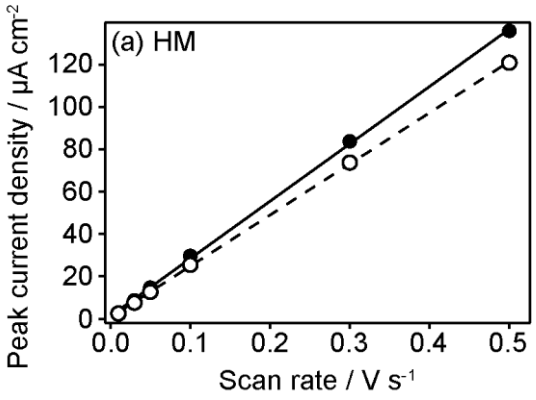
(a) HM
Peak current density / μA cm-2
Scan rate / V s-1
0
20
40
60
80
100
120
0.0
0.1
0.2
0.3
0.4
0.5

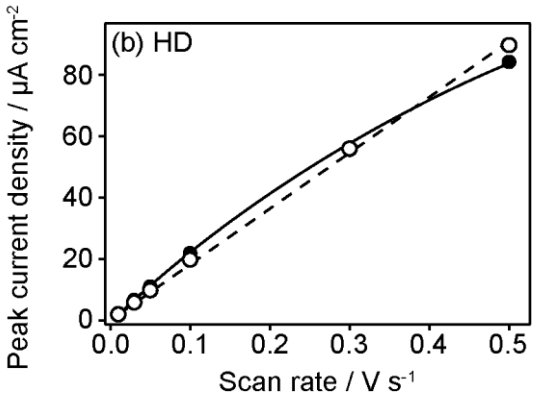
(b) HD
Peak current density / μA cm-2
Scan rate / V s-1
0
20
40
60
80
0.0
0.1
0.2
0.3
0.4
0.5

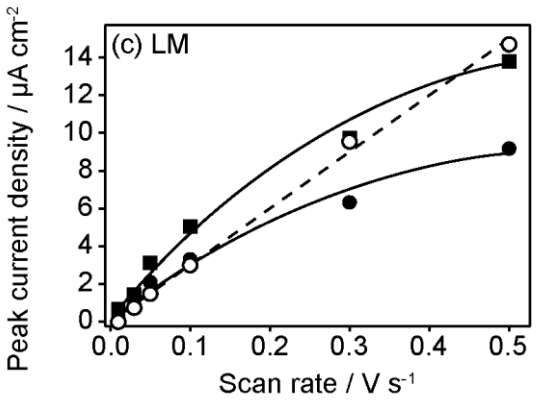
(c) LM
Peak current density / μA cm-2
Scan rate / V s-1
0
2
4
6
8
10
12
14
0.0
0.1
0.2
0.3
0.4
0.5

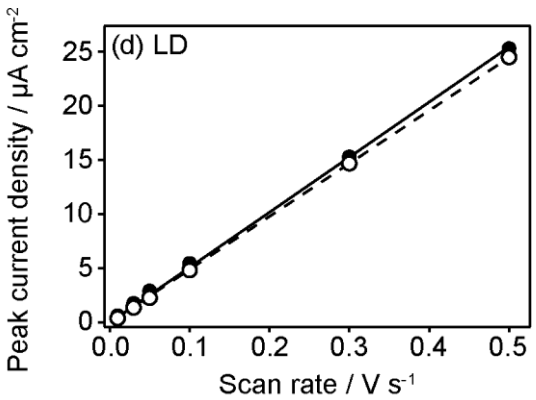
(d) LD
Peak current density / μA cm-2
Scan rate / V s-1
0
5
10
15
20
25
0.0
0.1
0.2
0.3
0.4
0.5

Figure 5 Plot of anodic (filled circle, solid line) and cathodic (open circle, dashed line) peak current densities on cyclic voltammograms (Figure 4) as a function of scan rate. The data for (c) LM sample has two anodic peak contributions; the pre-peak (filled square) and the post-peak (filled circle).

For HD sample, the anodic peak potential also shifted to become more positive (from +0.37 to +0.41 V *vs*. Ag/AgCl) with increasing sweep rate. As in the case of HM sample, this result corresponds to the presence of aggregated VFC molecules suggested from the AFM, XPS, and ellipsometric results of HD sample as already described. The FWHMs of the peaks for HD sample were also around 0.25 V, which are also broader than the ideal case. In addition, the anodic waves had a shoulder peak at around +0.28 V indicated by an arrow in Figure 4b, suggesting the presence of ferrocenyl groups with two different electrochemical environments: It is considered that the ferrocenyl groups which gave the main anode peak at +0.37 to +0.41 V suffer a larger repulsion among the positively charged ferricinium moieties when oxidized, while those having a more negative shoulder at +0.28 V suffer less repulsion; one is with a large repulsion among the positively charged ferricinium moieties and the other is with a rather small repulsion. Anodic peak currents did not show linear dependency on the scan rate, as shown in Figure 5b, also indicating that the presence of the aggregation prevents the anions from diffusing to the electrochemically active groups. The cathodic waves had only one peak while the anodic waves had two peaks. One plausible explanation for this is that the anions diffuse from the aggregation to the solution without much resistance. The two electrochemically active states mentioned above probably correspond to the surface aggregation and the underlying monolayer of

VFC, respectively, and it is indicated that the contribution from the aggregation is still large in this sample. The aggregation is also indicated by the particulate surface observed by AFM (Figure 3c). We should note, however, that the aggregation was suppressed by the use of *n*-decane instead of mesitylene, as confirmed by the much smaller peak area, smaller C / Fe ratio, thinner ellipsometric thickness and smaller particle size for HD sample compared to those for HM sample.

Each anodic wave for LM sample had two peaks (Figure 4c). The anodic peaks at the lower potential are indicated by an arrow in Figure 4c and those at the higher potential are hereafter referred to as the pre-peaks and the post-peaks, respectively. The anodic pre-peaks, post-peaks, and cathodic peaks were located at +0.26 to +0.28, +0.36 to +0.41, and +0.25 to +0.29 V *vs.* Ag/AgCl, respectively, depending on the sweep rate. These two peaks suggest the presence of two electrochemical states as introduced in the previous paragraph. This suggestion is also supported by the similarity of main peak positions and shoulder peak positions in anodic waves of LM sample to those of HD sample. The anodic post-peak potential shifted to positive, and the cathodic peak potential shifted to negative, with increasing sweep rate, while the anodic pre-peak potential did not change. The FWHMs of the cathodic peaks increased from +0.12 V to +0.25 V with increasing sweep rate, and these FWHMs were broader than that of the ideal case (i.e., 90.6 mV [57]) due to the repulsion among the positively charged ferricinium moieties when oxidized. The anodic pre-peak currents and the anodic post-peak currents did not exhibit a linear dependence on the scan rate, as demonstrated in Figure 5c. These behaviors indicate aggregation of VFC molecules as is also indicated by the AFM image (Figure 3d). We

should note that the aggregation was suppressed by the use of the visible light method instead of the heating method.

Unlike the cases of HM, HD, and LM samples, pairs of anodic and cathodic waves without shoulder peaks are observed in the CV for LD sample (Figure 4d). The anodic and cathodic peaks are located at +0.23 to +0.24 V and +0.22 to +0.23 V, respectively, for all the sweep rates. The peak separations are around 0.01 V for all sweep rates. Such small and constant peak separations are typical for surface absorbed redox species, the redox reactions of which do not include diffusions of reactant in the solution. Both the anodic and cathodic peak currents exhibited linear dependences on the scan rate, as shown in Figure 5d. This is also typical for the case of redox reactions without diffusions of redox species. These CV results indicated that the monolayer consisting of surface-confined VFC molecules had been successfully formed without aggregated features, as also indicated in the AFM image. The broader FWHMs than that of the ideal case are also due to the repulsion among the positively charged ferricinium moieties when oxidized.

The surface density of electrochemically active ferrocenyl groups on LD sample was estimated to be 1.4×10^{-10} mol cm^{-2} from the cathodic peak area of the CV curves. In contrast, the surface density of Si-H groups on the H-Si(111) surface was 1.30×10^{-9} mol cm^{-2}, which is simply calculated from the Si-Si bond length (0.2352 nm). The coverage of the VFC SAM is thus estimated to be 11%; here, we define the coverage as the percentage of surface Si atoms bonded to VFC molecules. Each VFC molecule is assumed to be attached to a different Si atom. Zhang et al. [16] recently

simulated the packing of long-chain alkyl monolayers on H-Si(111) and concluded that the optimized coverage was 50%. In the case of VFC, the coverage should be smaller than the alkyl monolayers even though VFC molecules are most closely packed, since a VFC molecule has a larger head group than a normal alkyl chain. From the diameter of the ferrocenyl group, 6.6 Å, the maximum density would be 4.5×10^{-10} mol cm^{-2} , i.e., 35% coverage [58]. Fabre et al. reported the density of 3.4×10^{-10} mol cm^{-2}, i.e., 26% coverage [48]. The surface density determined in this work is comparable to these values.

Here, we discuss our method for the fabrication of VFC monolayer. When comparing the activation processes, the visible light process is more advantageous than the heat treatment process. As described above, the heat treatment causes decomposition, or polymerization, of VFC molecules, and hence a particulate surface. One of the ferrocene derivatives, 4-ferrocenylbenzylalcohol, is reported to decompose above 200 ˚C [59]. VFC molecules probably decompose at 150 ˚C during the heat treatment used for fabricating HM and HD samples. As a solvent for VFC, *n*-decane is better than mesitylene. Aggregation of VFC molecules seemed to be suppressed in *n*-decane. One plausible explanation for the aggregation in mesitylene is as follows: A Si radical formed on a H-Si(111) sample surface might extract a H atom from a VFC molecule [10]. Consequently, some of the VFC molecules are converted to radicals. These radicals are stabilized in an aromatic solvent, through the formation of π-complex by coordination between the radicals and aromatic rings. Thus, the activation energy to form a VFC radical from a VFC molecule is lowered. This is why VFC molecules more readily polymerize in mesitylene than in *n*-decane. Among the four processes in

the present study, the best method was the combination of the visible light activation and the use of *n*-decane. By this method, the SAM was successfully formed from VFC molecules without aggregation. The C / Fe ratio of LD sample determined from the XPS analysis, i.e., 10.0, is a little smaller compared with the ideal value (i.e., 12). The reason for this is almost certainly a screening effect by the Fe atoms in the ferrocenyl groups. Photoelectrons from C atoms located underneath the ferrocenyl layer in the VFC-SAM are scattered by the Fe atoms to some extent. The static water contact angle of LD sample was 75.6˚, which is close to the reported value for the SAM formed from ferrocenethiols on Au substrate i.e., 64.5˚ [60], which also suggests successful uniform SAM formation from VFC molecules on H-Si(111) in this case.

3.2 Visible-light photo-responsivity of electrochemical behaviors

In this section the visible-light photo-responsivities of electrochemical behaviors of the VFC-SAM covered Si samples are investigated. To suppress the oxidation during the film formation, low-doped silicon wafers were used in the experiment in this section instead of high-doped Si wafers, and both n-type (Phosphorous doped, 1 - 10 Ω cm, single-side mirror-polished) and p-type (Boron doped, 1 - 30 Ω cm, single-side mirror-polished) silicon (111) wafers were used to compare the photo-responsivity. The LD method, which is considered to be the best way to form a VFC-SAM, was chosen as the formation method for the experiments in this section. The light intensity and the reaction time were set at 170 mW cm^{-2} and 4 hours, respectivily, for both n-type and p-type wafers.

The results obtained from the wettability measurement, XPS measurement and ellipsometric thickness measurement are summarized in Table 3. For the hydrogen-terminated n-type and p-type silicon, the oxygen content was smaller than for the hydrogen-terminated silicon obtained in the former section. This is because the low doped silicon has less defects and is less likely to be oxidized than the high doped silicon. The XPS Fe 2p spectra of both the n-type and p-type SAM-formed samples are displayed in Figure 6. Each spectrum has a peak at around 708.0 eV of binding energy and a sharp peak at about 720.9 eV. The former peak and the latter peak are attributed to be Fe $2p_{3/2}$ of two-valenced Fe and Fe $2p_{1/2}$ of two-valenced Fe. No peak contribution was found at around 712.0 eV for either spectrum, which would be attributed to Fe $2p_{1/2}$ of three-valenced Fe. The two-valenced Fe signal component implies the existence of Fc^{0+} and no three-valenced Fe signal component implies absence of Fc^{1+} or iron oxide (Fe_2O_3).

Table 3 Water contact angles, XPS quantitative analytical data, and ellipsometric thickness of hydrogen-terminated n-type and p-type silicon and the samples after film formation by optimized method.

		XPS quantitative analysis [at.%]					
	Water contact angle [˚]	Fe	C	O	Si	C / Fe ratio	Ellipsometric thickness [nm]
H-Si sample (n-type)	88.2	—	2.9	1.4	95.7	—	—
H-Si sample (p-type)	87.6	—	3.3	1.6	95.1	—	—
Film-formed sample (n-type)	77.2	1.9	17.4	9.5	71.2	9.2	1.54
Film-formed sample (p-type)	75.2	1.7	16.3	10.8	71.2	9.6	1.93

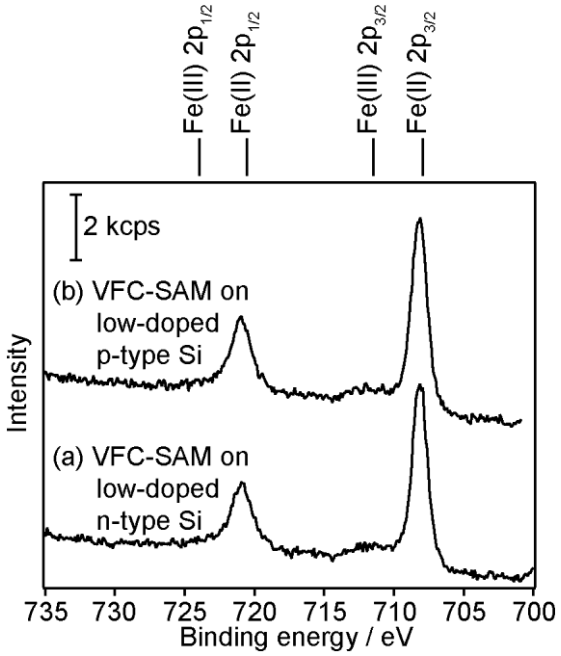

Figure 6 XPS Fe 2p spectra of samples after the reaction with vinylferrocene (VFC) by LD method on low-doped (a) n-type and (b) p-type slicon wafer.

The water contact angles of the two film-formed samples are both around 76° which is consistent with the value reported as ferrocene-terminated samples [54]. The thicknesses obtained for the two SAM-formed samples are similar to that of the LD sample described in the previous section, meaning that the thicknesses are around mono molecular size of VFC. The element content ratios obtained from XPS quantitative analysis for the both n-type and p-type film-formed samples were also the same value as for the LD sample in the previous section. The lower oxygen contents are obtained because the surfaces are less oxidized during the film formation treatment for low-doped silicon substrates than for high-doped silicon. The C/Fe ratios were 9.2 and 9.6 for the n-type and p-type film-formed samples, respectively, and are a little smaller

than the ideal value of 12. This may be explained by a screening effect of the signal from C atoms underneath the ferrocenyl group by the Fe atoms in the ferrocenyl groups.

AFM images obtained on the hydrogen-terminated samples and film-formed samples for n-type and p-type wafer are displayed in Figure 7. The two hydrogen-terminated silicons have a structure with terraces and steps, which is common for such samples, and both film-formed samples also have this structure, which means that the molecules are arranged with high orientation on the surface after film-formation treatment.

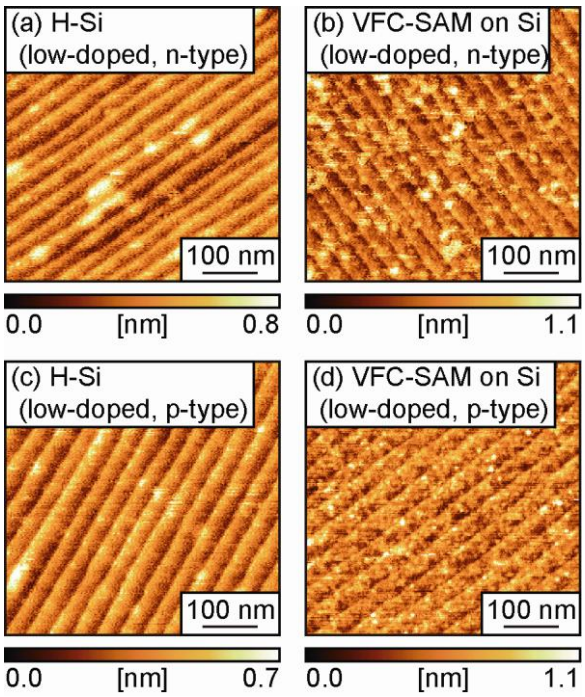

Figure 7 AFM topographic images of hydrogen-terminated Si(111) substrates (low-doped, (a) n-type (c) p-type) and VFC-SAM formed samples using the optimized method on (b) n-type and (d) p-type silicon wafers.

Electrochemical behaviors were observed using cyclic voltammetry (CV) with or without irradiation of the film-covered sample surface with a halogen lamp (PICL-NRX, Nippon PI) to examine the visible-light photo-responsivity. The intensity of the irradiated visible light was 6 mW cm^{-2} or 20 mW cm^{-2}. The observed CV graphs are shown in Figure 8. Figure 8a represents CV curves of the n-type film-formed sample obtained under 20 mW cm^{-2} illumination, and shows sets of anodic and cathodic waves. The peak potentials of each anodic and cathodic wave are around -0.09 and did not change. The peak separation width is less than 0.01 V. These features imply that the redox active species are adsorbed on the sample surface, and ferrocene moieties are tethered on the surface. The peak widths are all 0.25 to 0.28 V, which is larger than the ideal value of 0.091 V and implies that the coulomb interaction of ferrocenyl groups is not negligible. As shown in Figure 8b, the peak current densities of anodic waves are proportional to the scan rate, which also implies that the redox active species are adsorbed on the sample surface, and ferrocene moieties are tethered on the surface. Taking the results from AFM image on n-type film-formed sample into account, the obtained VFC-film is VFC-SAM. The density of VFC molecules immobilized on the surface of the n-type silicon surface is calculated to be 1.4×10^{14} cm^{-2} from the coulomb amount in the CV graph, and substitution rate from Si-H bond to Si-C bon d is *c.a.* 18%. Figure 8cd shows the CV graphs for n-type VFC-SAM-formed samples obtained in the dark and under illumination powers of 6 mW cm^{-2} and 20 mW cm^{-2}. Clearly, the sample shows photo-responsivity. Under dark conditions they did not show peaks. Under more intense illumination, all the

peaks shifted negatively. The discussions of this result are given later with the result for the p-type sample.

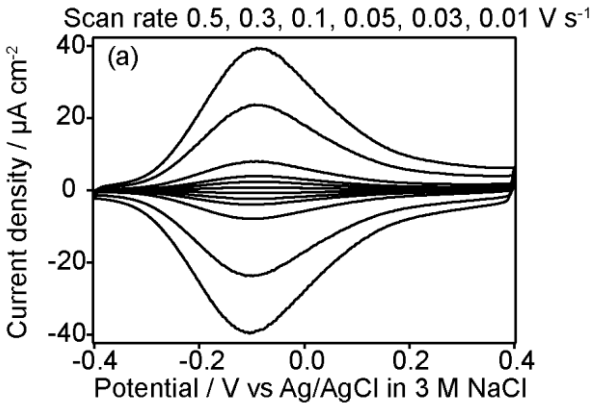
Scan rate 0.5, 0.3, 0.1, 0.05, 0.03, 0.01 V s-1
(a)
Current density / µA cm-2
Potential / V vs Ag/AgCl in 3 M NaCl

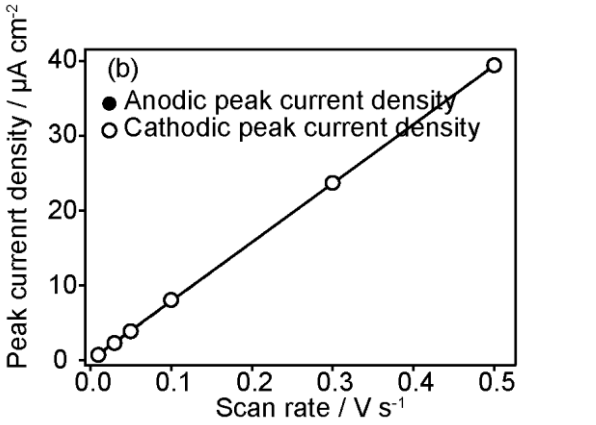
(b)
Anodic peak current density
Cathodic peak current density
Peak currenrt density / µA cm-2
Scan rate / V s-1

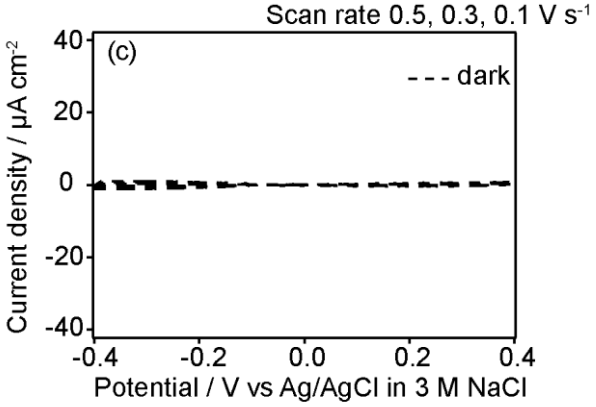
Scan rate 0.5, 0.3, 0.1 V s-1
(c)
dark
Current density / µA cm-2
Potential / V vs Ag/AgCl in 3 M NaCl

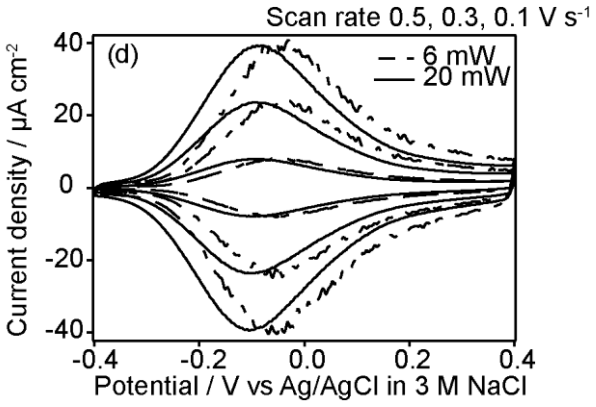
Scan rate 0.5, 0.3, 0.1 V s-1
(d)
6 mW
20 mW
Current density / µA cm-2
Potential / V vs Ag/AgCl in 3 M NaCl

Figure 8 Cyclic voltammograms for VFC-SAM formed samples on low-doped n-type Si wafer. The voltammograms were measured in aqueous 0.1 dm^{-3} $HClO_4$ solution at room temperature (a) under 20 mW cm^{-2} illumination, (c) in the dark, and (d) under 6 and 20 mW cm^{-2} illumination. Scan rates were (a) 0.01, 0.03, 0.05, 0.1, 0.3, and 0.5 Vs^{-1} and (cd) 0.1 to 0.5 Vs^{-1}. (b) Plot of anodic (filled circle, solid line) and cathodic (open circle, dashed line) peak current densities on cyclic voltammograms under 20 mW cm^{-2} illumination (Figure 8a) as a function of scan rate are also shown.

Figure 9a shows the CV curves for a p-type film-formed sample obtained in the dark. A set of anodic and cathodic waves are obtained, and the peak potentials are all around 0.29 V for all scan rates. The peak separations are all 0.01 V. The peak current densities of cathodic and anodic waves are proportional to the scan rate. These results imply that the redox active species are on the substrate surface. The FWHMs of the cathodic and anodic waves are 0.37 to 0.47 V, which are larger than the ideal value of 0.091 V because the coulomb interaction is not negligible. Taking the AFM result for the p-type film-formed samples into account, the formed VFC-film is VFC-SAM. The density of VFC molecules on the surface is calculated to be 4.4 x 10^{13} cm^{-2} from the coulomb amount in the CV graph, and substitution rate is calculated to be 5.6%. These molecular density and substitution rates are about one third those of the n-type film-formed samples, while the Fe amounts detected by XPS measurement are almost the same for the two samples. This may be because two thirds of the VFC molecules are not connected to the silicon bulk by Si-C linkage for the p-type film-formed sample, although they are immobilized on the surface with atomic

precision. Figure 9c shows the CV graphs for p-type film-formed samples obtained in the dark and under illumination powers of 6 and 20 mW cm^{-2}. All waves have a peak around 0.28 V, which is considered to come from the redox reaction of ferrocebyl groups. This reaction did not show photo-responsivity. This negative photo-responsivity for p-type film-formed sample will be discussed later. At -0.75 V, a peak was obtained under illumination. This peak showed photo-responsivity and a new cyclic voltammogram was obtained in the dark in the range below 0.4 V (Figure 9d). This peak showing photo-responsivity may come from the redox reaction of Fe^{2+} + 2e = Fe, for which the redox standard potential is -0.44 vs. NHE, that is, -0.24 vs. Ag/AgCl in 3M NaCl. However, we cannot offer further discussion on this point.

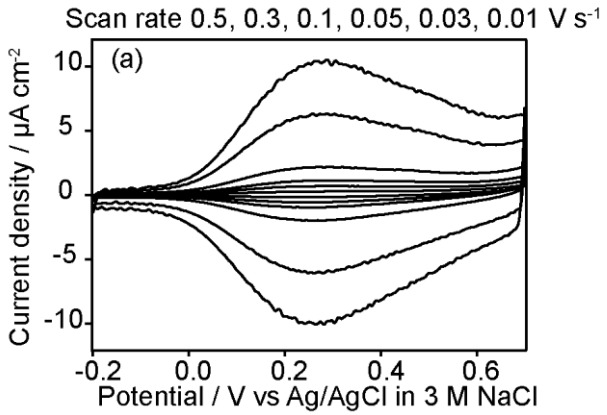
Scan rate 0.5, 0.3, 0.1, 0.05, 0.03, 0.01 V s-1
(a)
Current density / µA cm-2
Potential / V vs Ag/AgCl in 3 M NaCl

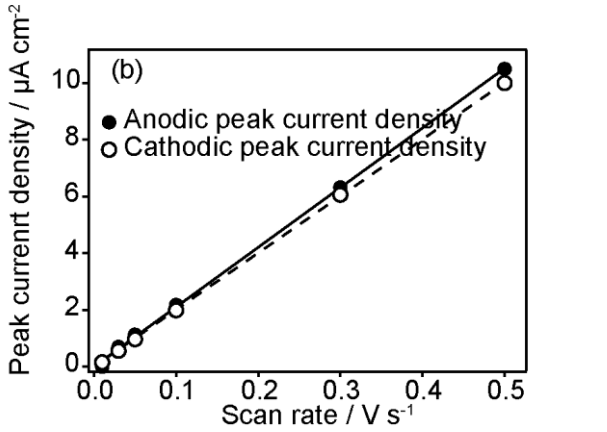
(b)
Anodic peak current density
Cathodic peak current density
Peak currenrt density / µA cm-2
Scan rate / V s-1

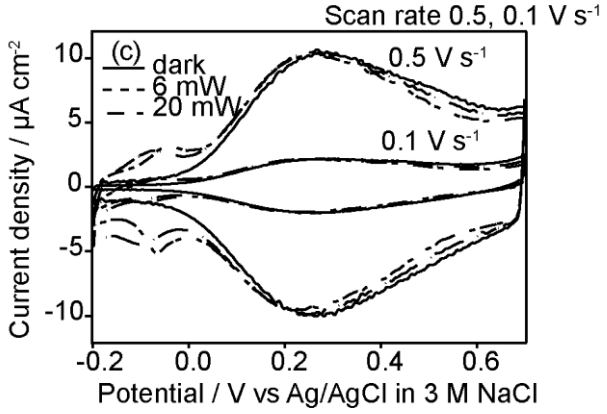
Scan rate 0.5, 0.1 V s-1
(c)
dark
6 mW
20 mW
0.5 V s-1
0.1 V s-1
Current density / µA cm-2
Potential / V vs Ag/AgCl in 3 M NaCl

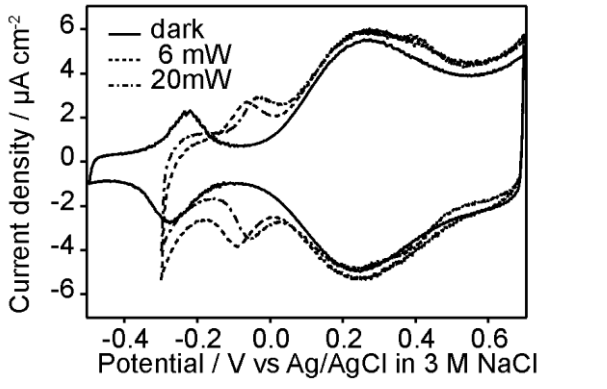
dark
6 mW
20mW
Current density / µA cm-2
Potential / V vs Ag/AgCl in 3 M NaCl

Figure 9 Cyclic voltammograms for VFC-SAM formed samples on low-doped p-type Si wafer. The voltammograms were measured in aqueous 0.1 dm^{-3} $HClO_4$ solution at room temperature (a,d) in the dark, and (c,d) under 6 and 20 mW cm^{-2} illumination. Scan rates were (a) 0.01, 0.03, 0.05, 0.1, 0.3, and 0.5 Vs^{-1}, (c) 0. 1 and 0. 5 Vs^{-1}, (d) 0. 5 Vs^{-1}. (b) Plot of anodic (filled circle, solid line) and cathodic (open circle, dashed line) peak current densities on cyclic voltammograms in the dark (Figure 9a) as a function of scan rate are also shown.

Now we will discuss the photo-responsivity of the reaction of ferrocene moities. This kind of photo-responsivity is often explained by considering the energy diagram at the interface of the molecule and silicon [28]. The energy diagram is drawn in Figure 10 with the following data: The conduction band and valence band of the silicon are -4.05 and -5.17 eV from vacuum level. The energy gap is 1.12 eV [61]. The highest occupied molecular orbital (HOMO) level of ferrocene molecule, which corresponds to the Fc/Fc^+ redox potential, is variously reported to be -4.5, -4.8, -5.1, and -5.4 eV from vacuum level [62-65]. These values are all around the valence band of silicon. The gap between HOMO and lowest unoccupied molecular orbital (LUMO) of the ferrocene moiety is experimentally obtained as described below. Figure 11 shows the visible light transmittance spectra of VFC solution and the peak at 440 nm is considered to be caused by the d-d transition of ferrocene moiety. The photon energy with the wavelength of 440 nm is calculated to be 2.8 eV and this is the HOMO-LUMO gap energy of ferrocene moiety. The LUMO level is 1.0-2.0 eV higher than the conduction band of silicon. For the energy diagram to be drawn as shown in Figure 10, the following three assumptions must be made: (1) Dipoles at the interface between

molecular film and silicon substrate are neglected. (2) The molecular orbit of the ferrocene moiety is not affected by the connections with the vinyl group and silicon substrate. (3) The HOMO level of ferrocene moiety is as high as or a little lower than the valence band of silicon. The third assumption denies any electron flow from HOMO in ferrocene to the valence band in silicon when no voltage is applied to the sample substrate, especially for the case of p-type film-formed sample.

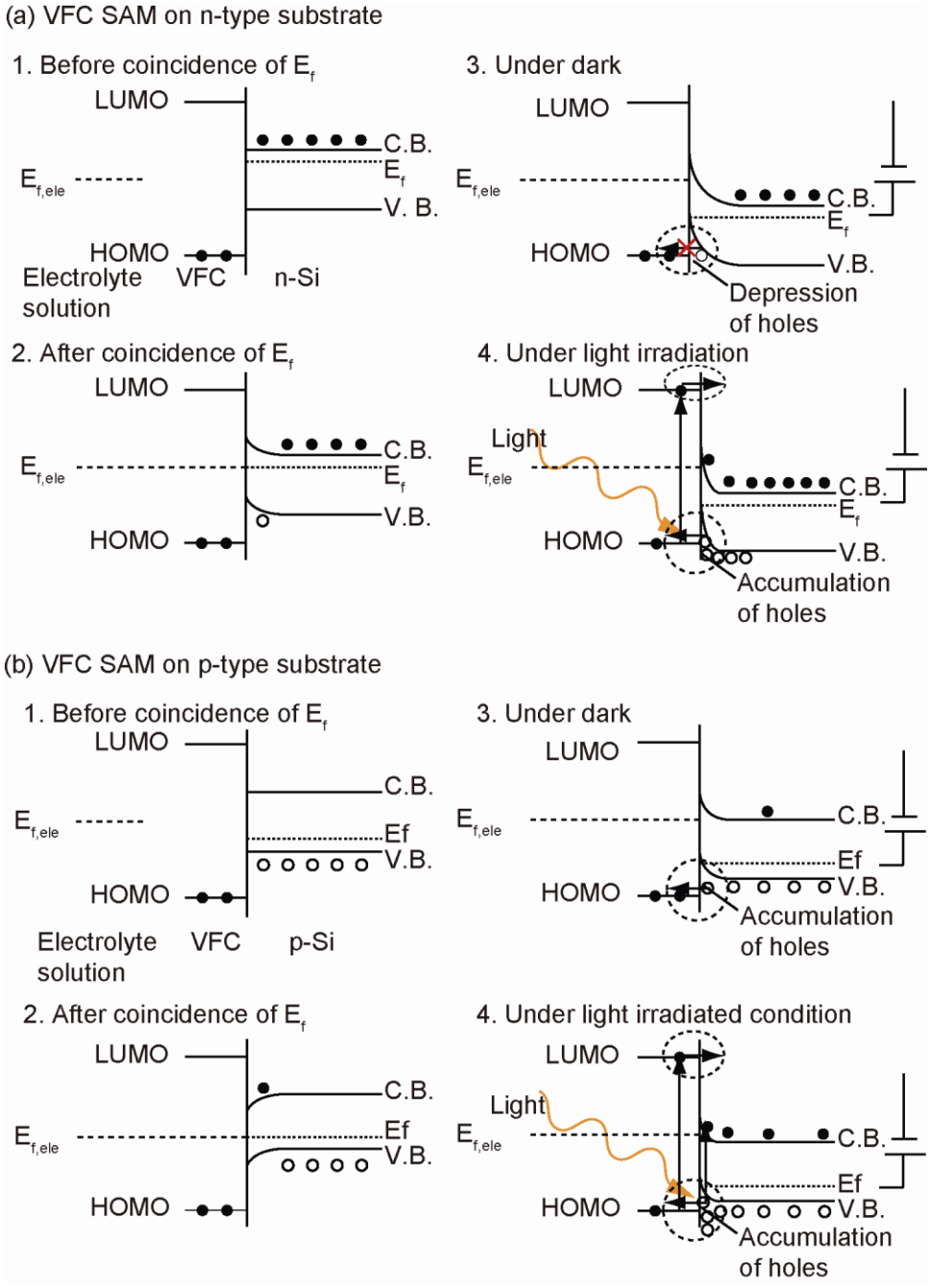

Figure 10 Energy diagram for VFC-SAM formed sample on the (a) n-type and (b) p-type silicon wafers. (a) For VFC-SAM on n-type substrate, no current flows in the dark, while current flows under light irradiation. The negative peak shift cannot be accounted for by this diagram. (b) For VFC-SAM on p-type substrate, current flows both in the dark and under illumination.

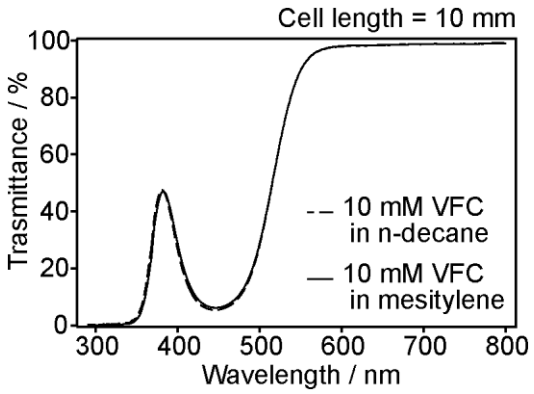

Figure 11 Visible light transmittance spectrum of 10 mM VFC in *n*-decane and mesitylene solution. The cell length is 10 mm.

For n-type film-formed sample in the dark, when the negative voltage was applied to the sample, the bands in silicon go down and the holes around the surface flow to the HOMO level of the ferrocene moiety. However, the holes are insufficient and the oxidation of the ferrocene moiety consequently does not continue. When the sample is illuminated, electron-hole pairs are generated and there a two-way flow of electron arises. One path is the flow of electrons from the HOMO level in ferrocene to the valence band in silicon resulting in hole-electron recombination. The second path is electrons in the HOMO level transitioning to the LUMO level in ferrocene by irradiated photons, and they flow to the conduction band in silicon. These flows are the rate-limiting factor of the ferrocene oxidation process, and photo-responsivity is observed for the n-type film-formed sample.

In contrast, for p-type film-formed sample, the holes in the valence band are always sufficient for electrons in the HOMO level in ferrocene to flow to the valence

band in silicon resulting in hole-electron recombination. Thus no photo-responsivity is observed for this sample.

4. Conclusions

Ferrocenyl-terminated films were formed on Si substrates through chemical reactions of VFC molecules with H-Si(111) surfaces. These films showed electrochemical activities indicating that the films were electrochemically linked to the Si substrates. In order to promote the chemical reactions of VFC with H-Si(111), we employed two methods. One was thermal activation by heating a Si substrate immersed in a VFC solution to 150 ˚C. The other was the visible light irradiation method. The latter was advantageous for the preparation of high quality SAM samples. Using the heat treatment process, many particulate deposits were formed on the sample surfaces probably due to aggregation of decomposed and/or polymerized VFC molecules, while with the visible light method the formation of such particulate deposits was highly suppressed. We also examined the solvent effects of mesitylene and *n*-decane, and confirmed that *n*-decane was a superior solvent for suppressing the particulate deposition of VFC. Consequently, by combining the visible light activation and the use of *n*-decane as a solvent, the deposits were suppressed almost completely and a uniform ferrocenyl-terminated SAM covalently bonded to Si was fabricated (LD sample). The C / Fe ratio estimated from XPS for the LD sample is close to the ideal value. From the areas of the cathodic wave in CVs of LD sample, by integrating the anodic and cathodic waves of the voltammograms for LD sample, the surface density of ferrocenyl groups was estimated to be 1.4×10^{-10} mol cm^{-2}, i.e., 11% in coverage.

We previously reported that heat treatment and visible light treatment give the same SAM when the molecules would not change their conformation [22]. In this paper, we showed a utilization example of visible light for SAM formation from molecules which are unstable under heat treatment. The visible light activation method will expand the options of precursor molecules for SAM formation to include those functional molecules which are usually unstable under heat treatment.

Finally we demonstrated the photo-responsivity of the electrochemical behavior of the resulting VFC-SAM formed sample on n-type and p-type silicon wafers. The sample on n-type silicon showed positive photo-responsivity, while the sample on p-type silicon showed negative photo-responsivity. The mechanism of the behavior is accounted for by describing the band diagram. These discussions should prove useful for the future design of minute photo-electronic devices.

Acknowledgment

This work was partially supported by a Grant-in-Aid for the Global COE Program, "International Center for Integrated Research and Advanced Education in Materials Science" and KAKENHI (B) No. 20360314, from the Ministry of Education, Culture, Sports, Science, and Technology of Japan.

References

[1] A. Ulman, An Introduction to Ultrathin Organic Films from Langmuir-Blogett to Self-Assembly, Academic Press, San Diego, CA, 1991.

[2] A. Ulman, Chem. Rev. 96 (1996) 1533.

[3] J. C. Love, L. A. Estroff, J. K. Kriebel, R. G. Nuzzo, G. M. Whitesides, Chem. Rev. 105 (2005) 1103.

[4] H. Sugimura, In: S. C. Tjong (Ed.) Nanocrystalline Materials: Their Synthesis-Structure-Property Relationships and Applications, Elsevier, Amsterdam, 2006, Chapter 3.

[5] P. R. Moses, R. W. Murray, J. Am. Chem. Soc. 98 (1976) 7435.

[6] T. Osa, M. Fujihira, Nature 264 (1976) 349.

[7] J. J. Sagiv, Am. Chem. Soc. 102 (1980) 92.

[8] S. R. Wasserman, Y. -T. Tao, G. M. Whitesides, Langmuir 5 (1989) 1074.

[9] M. R. Linford, C. E. D. Chidsey, J. Am. Chem. Soc. 115 (1993) 12631.

[10] M. R. Linford, P. Fenter, P. M. Eisenberger, C. E. D. Chidsey, J. Am. Chem. Soc. 117 (1995) 3145.

[11] J. M. Buriak, Chem. Rev. 102 (2002) 1271.

[12] D. D. M. Wayner, R. A. Wolkow, J. Chem. Soc. Perkin Trans. 2 (2002) 23.

[13] (a) C. P. Wade, C. E. D. Chidsey, Appl. Phys. Lett. 71 (1997) 1679. (b) C. P. Wade, C. E. D. Chidsey, Appl. Phys. Lett. 72 (1998) 133.

[14] A. B. Sieval, V. Vleeming, H. Zuilhof, E. J. R. Sudhölter, Langmuir 15 (1999) 8288.

[15] R. Boukherroub, S. Morin, P. Sharpe, D. D. M. Wayner, Langmuir 16 (2000) 7429.

[16] L. Zhang, K. Wesley, S. Jiang, Langmuir 17 (2001) 6275.

[17] M. P Stewart, J. M. Buriak, J. Am. Chem. Soc. 123 (2001) 7821.

[18] L. C. P. M. de Smet, G. A. Stork, G. H. F. Hurenkamp, Q. -Y. Sun, H. Topal, P. J. E. Vronen, A. B. Sieval, A. Wright, G. M. Visser, H. Zuilhof, E. J. R. Sudhölter, J. Am. Chem. Soc. 125 (2003) 13916.

[19] Q. -Y. Sun, L. C. P. M. de Smet, B. van Lagen, A. Wright, H. Zuilhof, E. J. R. Sudhölter, Angew. Chem. Int. Ed. 43 (2004) 1352.

[20] B. J. Eves, Q. -Y. Sun, G. P. Lopinski, H. Zuilhof, J. Am. Chem. Soc. 126 (2004) 14318.

[21] Q. -Y. Sun, L. C. P. M. de Smet, B. van Lagen, M. Giesbers, P. C. Thüne, J. van Engelenburg, F. A. de Wolf, H. Zuilhof, E. J. R. Sudhölter, J. Am. Chem. Soc. 127 (2005) 2514.

[22] H. Sano, H. Maeda, S. Matsuoka, K. -H. Lee, K. Murase, H. Sugimura, Jpn. J. Appl. Phys. 47 (2008) 5659.

[23] H. Sano, T. Yaku, T. Ichii, K. Murase, H. Sugimura, J. Vac. Sci. Tech. B 27 (2009) 858.

[24] Z. Liu, A. A. Yasseri, J. S. Lindsey, D. F. Bocian, Science 302 (2003)1543.

[23] L. Wei, D. Syomin, R. S. Loewe, J. S. Lindsey, F Zaera, D. F. Bocian, J. Phys. Chem. B 109 (2005) 6323.

[26] K. M. Roth, A. A. Yasseri, Z. Liu, R. B. Dabke, V. Malinovskii, K. -H. Schweikart, L. Yu, H. Tiznado, F. Zaera, J. S. Lindsey, W. G. Kuhr, D. F. Bocian, J. Am. Chem. Soc. 125 (2003) 505.

[27] Q. Li, G. Mathur, S. Gowda, S. Surthi, Q. Zhao, L. Yu, J. S. Lindsey, D. F. Bocian, V. Misra, Adv. Mater. 16 (2004) 133.

[28] S. Gowda, G. Mathur, V. Misra, Appl. Phys. Lett. 90 (2007) 142113.

[29] Q. Li, S. Surthi, G. Mathur, S. Gowda, V. Misra, T. A. Sorenson, R. C. Tenent, W. G. Kuhr, Z. Liu, D. F. Bocian, Appl. Phys. Lett. 83 (2003) 198.

[30] K. M. Roth, J. S. Lindsey, D. F. Bocian, W. G. Kuhr, Langmuir 18 (2002) 4030.

[31] P Kruse, E. R. Johnson, G. A. DiLabio, R. A. Wolkow, Nano Letters 2 (2002) 807.

[32] Q. Li, G. Mathur, M. Homsi, S. Surthi, V. Misra, V. Malinovskii, K. -H. Schweikart, L. Yu, J. S. Lindsey, Z. Liu, R. B. Dabke, A. Yasseri, D. F. Bocian, W. G. Kuhr, Appl. Phys. Lett. 81 (2002) 1494.

[33] Q. Zhao, Y. Luo, S. Surthi, Q. Li, G. Mathur, S. Gowda, P. R. Larson, M. B. Johnson, V. Misra, Nanotechnology 16 (2005) 257.

[34] E. A. Dalchiele, A. Aurora,; G. Bernardini, F. Cattaruzza, A. Flamini, P. Pallavicini, R. Zanoni, F. Decker, J. Electroanal. Chem. 579 (2005) 133.

[35] R. Zanoni, F. Cattaruzza, C. Coluzza, E.A. Dalchiele, F. Decker, G. Di Santo, A. Flamini, L. Funari, A.G. Marrani, Surface Science 575 (2005) 260.

[36] R. Zanoni, A. Aurora, F. Cattaruzza, C. Coluzza, E. A. Dalchiele, F. Decker, G. Di Santo, Flamini, A. Flamini, L. Funari, A. G. Marrani, Mat. Sci. Eng. C 26 (2006) 840.

[37] F. Decker, F. Cattaruzza, C. Coluzza, A. Flamini, A.G Marrani, R. Zanoni, E.A. Dalchiele, J. Phys. Chem. B 110 (2006) 7374.

[38] M. Cossi, M.F. Iozzi, A.G. Marrani, T. Lavecchia, P. Galloni, R. Zanoni, F. Decker, J. Phys. Chem. B 110 (2008) 22961.

[39] N. Tajimi, H. Sano, K. Murase, K.-H. Lee, H. Sugimura, Langmuir 23 (2007) 3193.

[40] R. Zanoni, M. Cossi, M. Iozzi, F. Cattaruzza, E. Dalchiele, F. Decker, A. Marrani, M. Valori, Superlattice. Microst. 44 (2008) 542.

[41] A. Boccia, A. Marrani, S. Stranges, R. Zanoni, M. Alagia, M. Cossi, M. Iozzi, J. Chem. Phys. 128, (2008) 154315.

[42] A. Marrani, E. Dalchiele, R. Zanoni, F. Decker, F. Cattaruzza, D. Bonifazi, M. Prato, Electrochim. Acta 53 (2008) 3903.

[43] A. Boccia, F. Decker, A. Marrani, S. Stranges, R. Zanoni, M. Cossi, M. Iozzi, Superlattice. Microst., 46 (2009) 30.

[44] K. Huang, F. Duclairoir, T. Pro, J. Buckley, G. Marchand, E. Martinez, J. Marchon, B. De Salvo, G. Delapierre, F. Vinet, ChemPhysChem 10 (2009) 963.

[45] A. Marrani, F. Cattaruzza, F. Decker, P. Galloni, R. Zanoni , Superlattice. Microst. 46 (2009) 40.

[46] S. Ciampi, P. Eggers, G. Le Saux, M. James, J. Harper, J. Gooding, Langmuir 25 (2009) 2530.

[47] B. Fabre, Accounts Chem. Res. 43 (2010) 656.

[48] B. Fabre, F. Hauquier, J. Phys. Chem. B 110 (2006) 6848.

[49] Y. J. Kim, J. Han, H. Sano, K. -H. Lee, K. Noda, T. Ichii, K. Murase, K. Matsushige, H. Sugimura, Appl. Surf. Sci. 256 (2009) 1507.

[50] H. Sugimura, A. Hozumi, T. Kameyama, O. Takai, Surf. Interface Anal. 34 (2002) 550.

[51] S. Kurokawa, T. Takei, A. Sakai, Jpn. J. Appl. Phys. 42 (2003) 4655.

[52] E. D. Palik, Handbook of Optical Constants of Solids, Academic Press, San Diego, CA, 1998, p. 547.

[53] E. A. Ambundo, M. -V. Deydier, A. J. Grall, N. Aguera-Vega, L. T. Dressel, T. H. Cooper, M.J. Heeg, L. A. Ochrymowycz, D. B. Rorabacher, Inorg. Chem. 38 (1999) 4233.

[54] Y. Sato, M. Maeda, Jpn. J. Appl. Phys. 33 (1994) 6508.

[55] C. M. Woodbridge, D. L. Pugmire, R. C. Johnson, N. M. Boag, M. A. Langell, J. Phys. Chem. B 104 (2000) 3085.

[56] H. Fukidome, M. Matsumura, Appl. Surf. Sci. 130-132 (1998) 146.

[57] A. J. Bard, L. R. Faulkner, Electrochemical Methods: Fundamental and Applications, 2nd ed.; Jhon Weiley & Sons, New York, 2001, p 590.

[58] C. E. D. Chidsey, C. R. Bertozzi, T.M. Putvinski, A. M. Mujsce, J. Am. Chem. Soc. 112 (1990) 4301.

[59] Z. Liu, A. A. Yasseri, J. S. Lindsey, D. F. Bocian, Science 28 (2003) 1543.

[60] J. A. M. Sondag-Huethorst, L. G. J. Fokkink, Langmuir 10 (1994) 4380.

[61] S. M. Sze, Semiconductor Device -Physics and Technology- 2nd ed., Wiley, New York, 1981.

[62] J. Pommerehne, H. Vestweber, W. Guss, R. F. Mahrt, H. Bassler, M. Porsch, J. Daub, Adv. Mater. 7 (1995) 551.

[63] G. Zhang, H. Zhang, M. Sun, Y. Liu, X. Pang, X. Yu, B. Liu, Z. Li, J. Comput. Chem. 28 (2007) 2260.

[64] M. G. Grigorov, J. Waber, N. Vulliermet, H. Chermette, J. M. J. Tronchet, J. Chem. Phys. 108 (1998) 8790.

[65] K. Seki, Mol. Cryst. Liq. Cryst. 171 (1989) 255.